Journal of Imaging Science and Technology® 55(1): 010201–010201-6, 2011.

Imbibition and Evaporation of Water Droplets on Paper and Solid Substrates

A. Oko and A. Swerin▲
YKI, Ytkemiska Institutet AB/Institute for Surface Chemistry, Box 5607, SE-114 86 Stockholm, Sweden
E-mail: agne.swerin@yki.se

P. M. Claesson
Department of Chemistry, Surface and Corrosion Science, Royal Institute of Technology, SE-100 44 Stockholm, Sweden

Abstract. *Imbibition and evaporation of picoliter (pL) sized water droplets on paper media commonly used for inkjet printing is measured using high speed imaging system. Three types of uncoated and coated paper samples were chosen: multipurpose uncoated paper* (80 g/m^2)*, matte coated paper* (230 g/m^2)*, and gloss coated paper* (240 g/m^2)*. As a reference, the rate of the evaporation process was quantified by using three impermeable solid substrates with different wetting characteristics, i.e., silicon, glass, and hydrophobized glass. It is shown that for water droplets of about 60 pL, imbibition is the dominant phenomenon on the matte and gloss coated paper leading to a total drying time (imbibition plus evaporation) of 10–15 ms for gloss coated paper and 30–150 ms on the matte coated paper. In the latter sample, different regimes in the imbibition process were correlated with the layered structure of the sample. The drying process on the multipurpose paper is dominated by evaporation, with initial drying rate of 0.4–0.6 pL/ms. © 2011 Society for Imaging Science and Technology.*
[DOI: 10.2352/J.ImagingSci.Technol.2011.55.1.010201]

INTRODUCTION

Dynamics of liquid imbibition are of special interest due to its industrial applications in, e.g., printing processes, and it also offers substantial fundamental research challenges. It is well established that the drying time of liquid droplets on a permeable substrate is set by the liquid evaporation rate and the imbibition rate and that the relative importance of these processes strongly depends on the substrate characters such as porosity and surface energy as well as on the degree of liquid volatility. When a liquid droplet is impinged onto a paper coated with a porous layer it experiences evaporation, expansion of the droplet base diameter, and imbibition into the porous matrix, as illustrated in Figure 1.

Capillary rise is described by the Lucas-Washburn (LW) equation. In the equation the height h of a liquid meniscus in a cylindrical capillary with a radius R is given by

$$h^2 = t\frac{2\sigma R\cos\theta}{2\mu}, \tag{1}$$

where t is time, σ is the liquid vapor surface tension, θ is the contact angle and μ is the liquid viscosity. The capillary rise described by Eq. (1) is dominated by the viscous force exerted by the rising liquid and by the Laplace pressure exerted by the curvature of the liquid meniscus. Other equations can be found describing regimes dominated by other forces[1–3] but discussion of their applicability is outside the frame of this work.

When imbibition is taking place in a complex porous network, the liquid is imbibing into numerous single capillaries of different length and cross sections with different chemistries (different contact angle θ). In this case, Eq. (1) cannot fully describe the process since, for example, most capillaries in porous networks do not have circular cross sections. Interconnectivity has to be taken into account and the presence of other chemical moieties such as binder may affect the liquid diffusion process.

The complexity of the pore network present inside many porous substrates necessitates consideration of simplified models when interpreting experimental results. For example, the average pore diameter of a real network can in a model be considered as a set of parallel capillaries with different radius and equal contact angle. This model is useful when long imbibition times are discussed (where viscous

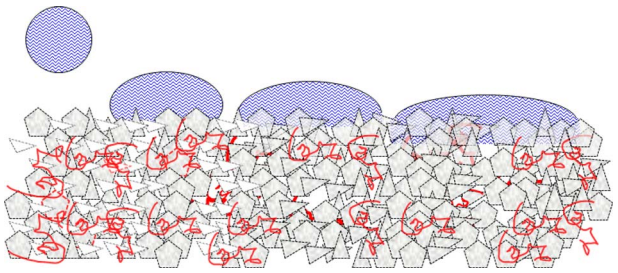

Figure 1. Illustration (not to scale) of spreading and imbibition of a liquid droplet (blue) impinged on a paper coated with a porous layer consisting of pigment particles (gray) of different shapes and a binder (red).

▲IS&T member

Received May 29, 2010; accepted for publication Aug. 24, 2010; published online Dec. 16, 2010.
1062-3701/2011/55(1)/010201/6/$20.00.

and gravitational forces are predominant) and the pore diameter distribution of the system can be considered as continuous.[4] In another model applicable for uniform porous media, a uniform advancing liquid front is assumed to exist inside the pore network, and a modified Lucas-Washburn equation is derived using parameters characterizing the real pore network, such as: porosity, specific surface area, contact angle, pore geometry, and tortuosity for a given system.[5,6] In a third more advanced model[7] the pore-network is considered as a unit cell made of a set of pores and connecting throats, which allows simulation of the resulting imbibition process.

Fig. 1 illustrates the expansion of the droplet base diameter immediately after the droplet surface impact. While expanding, additional surface area is engaged in the imbibition process. It is therefore useful to normalize the droplet volume by the droplet base surface area, giving an average length per surface area. This quantity will be referred to as the *effective length* h_{eff} and defined as

$$h_{\text{eff}}(t) = C + \frac{V_0 - V(t)}{\pi R_d^2(t)}, \tag{2}$$

where C and V_0 are correction terms (see appendix for further discussion), $V(t)$ is the droplet volume at time t, and $R_d(t)$ is the sessile drop base radius at time t. When imbibition takes place h_{eff} is related to the average distance between the surface and the advancing liquid front inside the porous network. However, the actual distance is not equal to h_{eff} since Eq. (2) does not take into account the porosity of the medium, tortuosity of the liquid passage inside the porous medium, and imbibition taking place parallel to the surface (wicking).[8]

The dimensions of small droplets with a diameter of few mm or less have significant role on setting the evaporation rate when volatile liquids are considered. Hu and Larson[9] derived a simple expression describing the net evaporation rate $\dot{m}(t)$ (g/s) of a sessile drop with a contact angle (CA) less than 90°:

$$\dot{m}(t) = -\pi r(t) D \left(1 - \frac{RH}{100}\right) c_v [0.27\theta(t)^2 + 1.3], \tag{3}$$

where $r(t)$ (mm) is the measured base radius of the sessile drop at time t (contact line radius), D (mm^2/s) is the water vapor diffusivity, RH (%) is the relative humidity, c_v (g/mm^3) is the saturated water vapor concentration, and $\theta(t)$ (rad) is the measured CA at a time t. The strong dependency of $\dot{m}(t)$ on $r(t)$ and the weak dependency on $\theta(t)$ is a result of high vapor flux at the perimeter of the droplet base (three phase contact line) regardless of the CA value.[9]

MATERIALS AND METHODS

Silicon wafers and microscope glass slides used for the evaporation measurements were washed several times by purified water (Milli-Q plus unit, Millipore USA) and acetone (Solveco, Sweden). Hydrophobized glass surfaces were prepared by first washing microscope glass slides in ethanol and acetone. The glass slides were then immersed for 15 min in a water-hydrogen peroxide solution, followed by rinsing with purified water. In the next step, the surfaces were immersed in water: hydrogen peroxide: ammonium hydroxide solution with the composition ratio 5:1:1. The hydrophobization was carried out in the gas phase by placing the microscope slide over night in a desiccator together with a glass Petri dish containing a few drops of 1H,1H,2H,2H-perfluorodecyltrichlorosilane, 96% (Alfa Aesar, Germany).

Three types of commercially available paper samples were used: uncoated multipurpose home and office paper (80 g/m^2, M-real, Sweden), matte coated (230 g/m^2, photo supreme double-sided matte, Staples, USA) and gloss coated (240 g/m^2, photo plus gloss, Staples, USA).

Cobb_{60} values were obtained according to ISO 535:1991. Five measurements were performed on each type of paper and the average values were calculated.

Liquid imbibition measurements were made using a DataPhysics OCA40 micro (DataPhysics GmbH, Germany) capable of delivering droplets with volumes in the tens of picoliter (pL) range. The system includes a high-speed charge coupled device camera (maximum 2200 images/s) with 50× magnification, a piezoelectric dispenser (marked "dispenser" hereafter, Microdrop GmbH, Germany) that delivers single 60 pL water droplets with a speed of 1.5 m/s, and a Peltier sample stage for accurate control of the temperature. In all experiments the temperature and relative humidity were kept constant at 23±1°C and 45±3%, respectively. In the analysis, a solid liquid baseline is set manually for each recorded sequence and then the analysis is done automatically by the SCA 20 software. For the volume calculation it is assumed that the droplets take the shape of a spherical cup. Images of the surfaces in air were recorded using an atomic force microscope (combined confocal Raman microscope/AFM/SNOM alpha300 RAS, WITec, Germany) in tapping mode using noncontact cantilevers with a spring constant of 42 N/m.

X-ray photoemission spectroscopy (XPS) measurements were carried out by using a Kratos AXIS $\text{Ultra}^{\text{DLD}}$ x-ray photoelectron spectrometer (Kratos Analytical, Manchester, UK). The samples were analyzed using a monochromatic Al X-ray source operated at 150 W (10 mA/15 kV). The analysis area was below about 1 mm^2 (with most of the signal from an area of 700×300 μm). In the analysis, low resolution wide spectra (pass energy 160 eV) was used to quantify the relative amounts of elements, and quantification of the different types of carbons (C1-C5) was done by deconvolution of high resolution carbon spectra (pass energy 20 eV) using known values for carbon chemical shifts (relative to the carbon peak at 285 eV): 0 eV for C1-carbon (C—C, C═C and C—H functional groups), 1.4–1.7 eV for C2-carbon (C—O or C—O—C), 2.7–3.3 eV for C3-carbon (O—C—O or C═O), 3.7–4.4 eV for C4-carbon (O—C═O or C(═O)OH), and 4.9–5.1 for C5-carbon (Ca-carbonate).

Scanning electron microscopy (SEM) images were taken

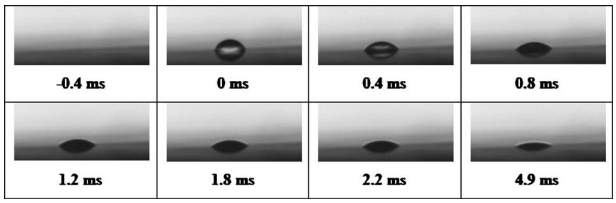

Figure 2. A sequence of images showing a droplet impinged on a gloss coated paper. The observed droplet volume at $t=0$ ms was 49 pL.

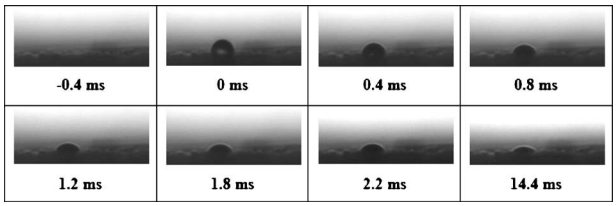

Figure 3. A sequence of images showing a droplet impinged on a matte coated paper. The observed droplet volume at $t=0$ ms was 41 pL.

using JEOL JSM-7000F and JEOL JSM-7401F, in a low landing energy (0.8–1.3 keV, in gentle-beam mode). The sample area in the images was not metal coated.

RESULTS

Below we will quantitatively analyze the change in droplet volume on porous paper substrates and solid substrates. This was done by analyzing a sequence of droplet images, and two typical image sequences are illustrated in Figures 2 and 3.

Paper Substrates

Chemical composition of the gloss coated paper surface measured by XPS (Table I) reveals a surface enriched in alumina pigments and binder (most probably poly(vinyl alcohol) or gelatin). The surface roughness [Figure 4(c)] exhibiting rms 70 nm and peak to peak (PP) value of 550 nm (Table I) resulting in a well defined baseline as seen from Fig. 2. The porous surface is visualized by SEM in Figures 5(a)–5(c). The exact pore size and distribution cannot be determined but the range of pore diameter can be estimated to be less than 100 nm. In Figure 6 the effective length and the droplet base diameter of three droplets impinged on different spots are plotted against the square root of time, together with linear curves fitted to the effective length data. In the fitting process the first three experimental points in each droplet sequence are excluded. For all three droplets, the points at 0 ms and to some extent the ones at 0.4 ms diverge from the fitted curves. The total observed drying time is similar for all droplets and measured to be 13–16 ms. In all droplets it takes about 1.2 ms after initial paper-droplet contact for the base diameter to reach its maximum value.

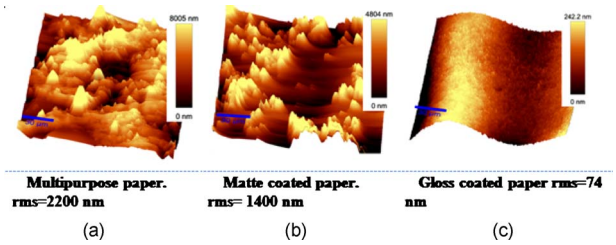

Figure 4. AFM images of paper surfaces. Note the difference in scale bars in the height direction.

Chemical composition of the matte coated paper surface determined by XPS (Table I) reveals a significant content of silicon atoms in the surface layer due to enrichment of silica gel aggregates in the coating layer. This sample exhibits a rough surface with rms roughness of 1400 nm and PP value of 13,000 nm [Table I, Fig. 3 and Fig. 4(b)]. SEM images [Figs. 5(b) and 5(d)] reveal two distinct pore populations, interaggregate and intra-aggregate. The interaggregate pores occur as a consequence of the gaps between the silica gel aggregates [Fig. 5(b)], while the intra-aggregate pores are voids inside the aggregates themselves [Fig. 5(d)]. The difference in pore size between the two distinct pore populations is estimated to be two orders of magnitude. The time evolutions of the base diameter and the effective length on droplets on the matte coated paper are shown in Figure 7. The droplet base diameter expansion period is similar to the one on the gloss coated paper, lasting about 1.2 ms. No linear curved are fitted to the effective length data, but a trend is seen in all droplets where the linear coefficient describing the rate of change in the effective length decreases after about 1.8–2.2 ms (Fig. 7, inset) and at an effective length of 6–11 μm. The sample exhibits the highest $Cobb_{60}$ value (45 g/m^2), and total drying times ranging between 30–100 ms, which are larger than those observed on the gloss coated paper (13–16 ms).

Table I. Surface characterization of the paper substrates. Roughness (rms and peak-to-peak, PP) values obtained from AFM, average $Cobb_{60}$ values and surface chemical composition (atomic percent) of the main elements detected by low and high resolution XPS analysis. C1 denotes aliphatic carbon and C2–5 all other types of carbons, mostly covalently bound to oxygen (see methods for further details).

Paper sample	Roughness rms (nm)	Roughness PP (nm)	Average $Cobb_{60}$ (g/m^2)	Surface chemical composition in atomic percentage (%)							
				O	N	Ca	Si	Al	C	C1	C2–5
Gloss coated	74	550	30	58				25.0	16	7.2	8.8
Matte coated	1400	13,000	45	39	3.2		14.0		42	24	18
Multipurpose	2200	19,000	28	36	0.9	0.9	0.2	<0.1	61	14.5	46.5

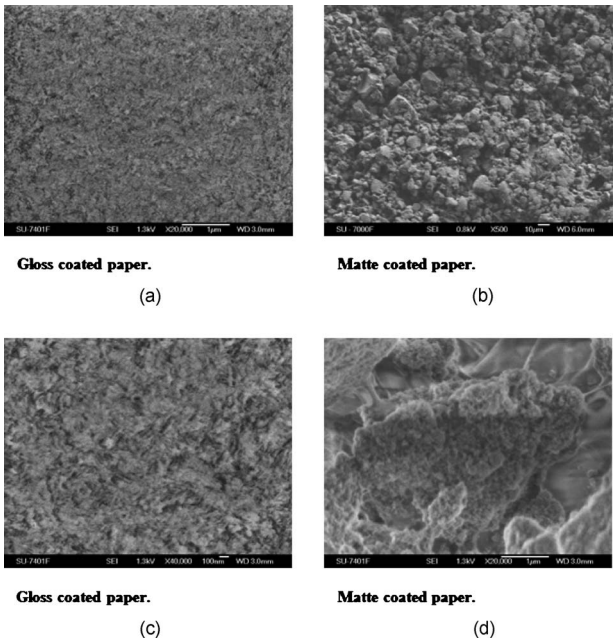

Figure 5. SEM images of gloss and matte coated paper samples. Note the different scale bars.

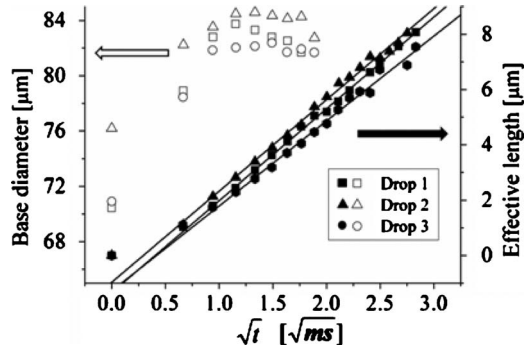

Figure 6. Effective length (filled symbols) and base diameter (unfilled symbols) in micrometers (μm) vs $\sqrt{t}(\sqrt{\text{ms}})$ for three separate droplets impinged on glass coated paper. The black lines are linear fits to the data.

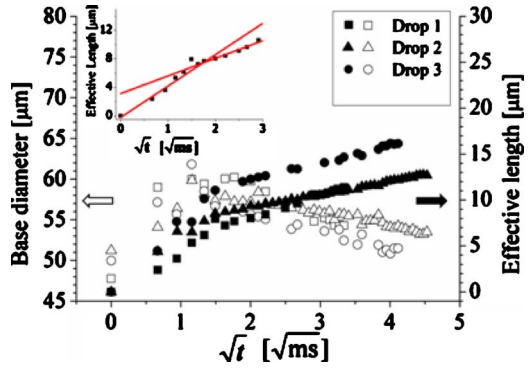

Figure 7. Effective length (filled symbols) and base diameter (unfilled symbols) in micrometers (μm) vs $\sqrt{t}(\sqrt{\text{ms}})$ for three separate droplets impinged on matte coated paper. The inset shows trend lines marking the two regions displaying differences in linear coefficient of imbibition vs $\sqrt{t}$.

Table II. Initial droplet drying rate and total drying time on multipurpose paper.

	Initial drying rate (pL/ms)	Total drying time (s)
Drop 1	0.05	1.1
Drop 2	0.06	1.0
Drop 3	0.04	1.3

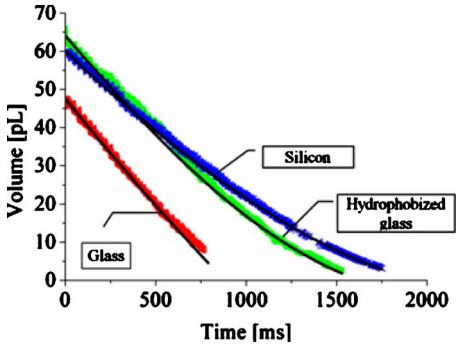

Figure 8. Volume loss in picoliters (pL) vs time (ms) on multipurpose paper.

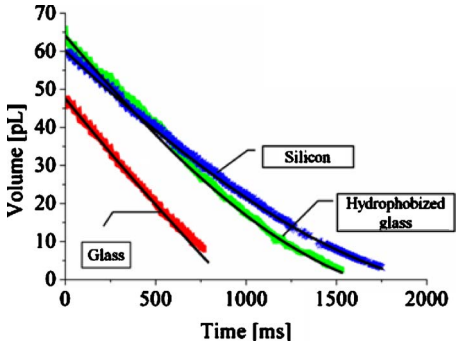

Figure 9. Volume loss in picoliters (pL) vs time (ms) on silicon (blue), glass (red) and hydrophobized glass (green) substrates. The black lines are obtained by fitting Eq. (3) to the measured data.

The multipurpose uncoated paper surface has a significant roughness as seen in Fig. 4(a), with rms equals 2200 nm and PP value of 19,000 nm (Table I). Volume loss data versus time is shown in Figure 9. The data exhibit time scaling, initial drying rates, and total drying times similar the ones observed on the impermeable substrates (see Table II and Figures 8 and 9), giving a clear indication that the evaporation process occurs much faster than the imbibition process. In contrast to the short time behavior, at long times and high volumes this sample exhibit high absorbance as reflected by the Cobb_{60} value of 28 g/m^2 (Table I). Chemical analysis of the paper surface carried out by XPS (Table I) reveals a surface enriched with carbon (61%) and oxygen (36%), as expected from the high cellulosic fiber content.

Solid Substrates: Evaporation Experiments

Initial evaporation rate (calculated from a linear fit to the initial points in each sample) and total drying time on the

Table III. Relaxed contact angle (obtained after initial spreading) and results from the evaporation of water droplets on impermeable samples.

Sample	Relaxed contact angle (deg)	Fitted RH (%)	Initial evaporation rate (pL/ms)	Initial droplet volume (pL)	Total observed evaporation time (s)	Linear correlation parameter, r^2
Hydrophobized glass	74	52	0.04	66	1.7	0.9995
Glass	40	50	0.05	48	1.0	0.9995
Silicon	80	61	0.03	59	2.0	0.9999

solid substrates range between 0.03–0.05 pL/ms and 1–2 s, respectively (Table III). Evaporation rate on the solid substrates together with fitted curves of Eq. (3) are shown in Fig. 9. Fitting was done by numerically integrating Eq. (3) (Ref. 9) with respect to time, where the experimental values of $r(t)$ and $\theta(t)$ were used, and taking $D=26.1$ mm^2/s and $c_v=2.32(10^{-8}$ g/mm^3), which were the same values used in Ref. 9 and obtained from the CRC handbook[10] for temperature of 25°C. The *RH* was varied until the best correlation was found. As seen from the correlation parameters and Fig. 9, there is an excellent agreement between the experimental data and the fitted curves. *RH* values obtained from the fit ranges between 50–61 % (Table III) which is slightly higher than the laboratory humidity (45±3%). It is noted that although the laboratory *RH* is well controlled, the *RH* value experienced by the droplet is significantly different due to evaporation of water from within the dispenser that increases the local *RH*. Such increment was verified by a simple experiment. The temperature of the sample stage was gradually lowered, until at 15.4°C water started to condense on the sample area precisely under the dispenser. Then the sample stage was slowly moved sideways resulting in a fresh dry area that came beneath the dispenser and was immediately covered by newly condensed liquid. At the same time, the wet area previously under the dispenser became dry almost instantly. As further confirmation, a different fitting procedure was chosen where the diffusion coefficient *D* was fitted instead of the *RH* value, resulting in unreasonably low *D* values, ranging from 18.1 mm^2/s for the clean silicon sample, 23.0 mm^2/s for the hydrophobized glass, and 23.1 mm^2/s for the clean glass.

DISCUSSION

Both the matte coated and multipurpose paper samples exhibit roughness values in the order of tens of μm, close in magnitude to the droplet base diameter (around 60 μm in this case). This is obviously a complication common to many surfaces of practical interest. Due to the high roughness of the surface the solid-liquid baseline is by necessity ill-defined, and there will be some distortions of the droplet symmetry. It is thus significant to ask if one can establish a typical droplet evaporation and imbibition rate on such substrates using pL droplets. Our results show that repeating the experiment on different spots gave similar results in terms of drying time and rate, as shown in Table II, Fig. 7 (matte coated paper), and Fig. 8 (multipurpose paper).

Initial droplet spreading stage lasts about 1–2 ms on both the matte and the gloss coated papers (Figs. 6 and 7), despite the significant differences in surface chemistry and roughness of the two (Table I). Comparing the total drying time on these two samples (10–100 ms) to the total evaporation time observed on the impermeable substrates (1–2 s, Table III), suggesting a much faster imbibition of water into the porous bed than evaporation. Consequently, subtracting the evaporation component from the experimental drop volume hardly affected the outcome of the analysis (data not shown).

The linear curves in Fig. 6 (gloss coated sample) suggest a LW type of imbibition, with a possible contribution by diffusion processes arising from interactions between water and molecular moieties in the coating layer (e.g., binder, surfactants, and salts). The reason behind the repeated divergence from the fitted linear curve, by the first and to some extent by the second experimental point in each sequence remains to be explained.

The matte coated sample exhibits total drying times with a wider span relative to the ones observed on the gloss coated paper (30–100 ms relative to 10–13 ms, respectively), which is a consequence of the much larger structural and most probably chemical heterogeneities of the matte coated paper (Fig. 5). The trend with a decrease in the linear coefficient describing the rate of change in the effective length versus $\sqrt{t}$ (Fig. 7) is particularly interesting. This can be rationalized by the LW equation [Eq. (1)] and taking into account the two distinct pore populations mentioned above, as well as the layered structure of the coating. The LW equation predicts a faster imbibition into large pores than into small ones with the same surface energy. In the matte coated sample the pore size difference between the two pore populations is two orders of magnitude. Consequently, in the initial few milliseconds most of the imbibition takes place in the large interaggregate pores, and hardly any in the small intra-aggregate pores. Once the liquid front reaches the end of the silica gel aggregate layer, most of the large pores are filled and imbibition takes place mostly inside the small, intra-aggregate pores, which is suggested to result in the smaller linear coefficient describing the change in effective length versus $\sqrt{t}$. Support for this scenario can be found in the similarity between the effective length associated with the decrease in linear coefficient (6–11 μm) and the thickness of the silica gel aggregate layer estimated by the aggregates size [about 1–15 μm, Fig. 5(b)] and the measured roughness PP value (13 μm, Table I).

Changes in the interior pore network structure may occur when water are absorbed by a media susceptive to swell-

ing, such as paper. It is reasonable to assume that any swelling experienced by one of the components inside the paper would result in out of plane deformation of the paper surface. Since no such deformation was observed in any of the samples, it was assumed that no significant change in the interior structure occurred during the impingement of pL water droplets.

The observation that no significant imbibition is experienced on the multipurpose paper is somewhat unexpected since this sample is hydrophilic and water absorptive as reflected by the Cobb_{60} value of 28 g/m^2. Delays in water uptake by paper were reported as early as 1967 by Bristow[11] and later by others (cited in Ref. 12). The hindered water imbibition can originate from the paper fibrous structure. Imbibition inside fibrous network can take place if liquid is allowed to transport in the form of continuous liquid columns that are confined by the fiber walls. In a simple representation fibers can be modeled as circular cylinders, for which it was shown[13] that liquid columns are susceptible to breakage even when the cylinders (fibers) are hydrophilic (contact angle $<90°$), resulting in formation of sessile drops that stop or significantly retard the imbibition process. The disagreement between the Cobb_{60} value and the lack of imbibition is an outcome of the differences between the Cobb measurement and impingement of pL droplets. The first reflect long time (tens of seconds) absorbance under hydrostatic pressure while the latter relates to much shorter times (ms to s) and volumes with negligible hydrostatic pressure.

CONCLUSIONS

In this work drying rates of pL-sized droplets on uncoated and coated paper were measured and analyzed. As reference, evaporation rates were measured on solid flat surfaces. The ability to distinguish between different drying kinetics on common inkjet media is enabled due to the combination of fast imaging and impingement of pL droplets. It was found that imbibition rather than evaporation dominated the drying process on coated paper samples, while evaporation dominates on the uncoated paper sample. Evaporation is a relatively slow process, and in the case of flat solid surfaces good agreement is found with predictions. Imbibition into the matte and gloss coated paper substrates is a significantly faster process, providing a linear relation between the change in effective length and the square root of time that implies a Lucas-Washburn type of imbibition. In the case of the gloss coated paper, only one linear coefficient is observed, while in the case of the matte coated paper, two linear coefficients can be distinguished. In the latter case, we suggest that the first linear coefficient arises due to the dominating imbibition in the interaggregates pore population at short time scales, and the second linear coefficient arises due to imbibition in the smaller intra-aggregate pore population that dominates at longer time scales. The clear time scale difference between the evaporation and imbibition or diffusion processes observed in this study is not general but will depend on the nature of the specific sample.

ACKNOWLEDGMENTS

The grant from Nils and Dorthi Troëdsson Foundation for the combined Raman/AFM equipment, and the grant from Knut and Alice Wallenberg Foundation for the XPS instrument are gratefully acknowledged. The authors thank Mikael Sundin (YKI) and Marie Ernstsson (YKI) for running the XPS and helping in interpretation, Birgit Brandner (YKI) for running the AFM, Norbert Heil (DataPhysics, Germany) for the technical support of the OCA40 Instrument, and Kjell Jansson (Department of Material and Environmental Chemistry, Stockholm University) for helping with the SEM imaging. The investigation is part of the NextJet research project, funded by industry and VINNOVA (Swedish Government Agency for Innovation Systems) in the forestry-based sectoral research program.

APPENDIX

Equation (2) reads $h_{\text{eff}}=C+[V_0-V(t)]/[\pi R_d^2(t)]$, where h_{eff} is the effective length, $R_d(t)$ is the droplet base radius at time t, $V(t)$ is the droplet volume at time t, and C and V_0 are two terms discussed below. h_{eff} is proportional to the difference between V_0 and $V(t)$, and inversely proportional to the droplet base area given by $\pi R_d^2(t)$. In the case where only one linear coefficient is observed (as on the gloss coated paper, Fig. 6) $C=0$ and V_0 is the initial experimental volume at $t=0$ (captured in the first frame). When two linear coefficients are observed (matte coated paper, Fig. 7), in the first stage corresponding to the first linear coefficient, $C=0$, and V_0 is the first experimentally observed volume, i.e., $V_0=V(t=0)$. At a time t_2, the second stage starts, corresponding to the second linear coefficient. Here V_0 is the volume observed at the start of the second stage, i.e., $V_0=V(t=t_2)$, and C is an offset term that equals the effective length calculated at $t=t_2$ (start of the second stage) but with $V_0=V(t=0)$ (the volume captured at $t=0$, the start of the first stage). This procedure is justified by the assumption that the second stage is dominated by imbibition in the small intra-aggregate pores.

REFERENCES

[1] N. Fries and M. Dreyer, J. Colloid Interface Sci. **327**, 125–128 (2008).
[2] B. V. Zhmud, F. Tiberg, and K. Hallstensson, J. Colloid Interface Sci. **228**, 263–269 (2000).
[3] D. Quéré, Europhys. Lett. **39**, 533–538 (1997).
[4] A. Marmur and R. D. Cohen, J. Colloid Interface Sci. **189**, 299–304 (1997).
[5] S. Gruener, T. Hofmann, D. Wallacher, A. V. Kityk, and P. Huber, Phys. Rev. E **79**, (2009).
[6] A. Marmur, Langmuir **19**, 5956–5959 (2003).
[7] C. J. Ridgway and P. A. C. Gane, Colloids Surf., A **206**, 217–239 (2002).
[8] R. C. Daniel and J. C. Berg, Adv. Colloid Interface Sci. **123–126**, 439–469 (2006).
[9] H. Hu and R. G. Larson, J. Phys. Chem. B **106**, 1334–1344 (2002).
[10] D. R. Lide, *CRC Handbook of Chemistry and Physics*, 79th ed. (CRC Press, Boca Raton, FL, 1998).
[11] J. A. Bristow, Sven. Papperstidn. **70**, 623–629 (1967).
[12] M. B. Lyne, in *Handbook of Physical Testing of Paper*, edited by M. B. Lyne, J. Borch, et al. (Marcel Dekker, New York, 2002), Vol. **2**, pp. 303–332.
[13] D. Lukás, J. Chaloupek, E. Kostáková, N. Pan, and I. Martinková, Physica A **371**, 226 (2006).